DOI: 10.1002/ejic.200901080

Synthesis and Characterization of 1-, 2-, and 3-Dimensional Bimetallic UO_2^{2+}/Zn^{2+} Phosphonoacetates

Karah E. Knope[a] and Christopher L. Cahill*[a]

Keywords: Hydrothermal synthesis / Uranium / Zinc / Heterometallic complexes / Organic–inorganic hybrid composites

Four bimetallic UO_2^{2+}/Zn^{2+} phosphonoacetates have been prepared from hydrothermal reactions of uranyl nitrate, zinc nitrate, and triethyl phosphonoacetate. These compounds, $(UO_2)_2(PPA)_2(H_2O)_2{\cdot}Zn(H_2O)_6{\cdot}4H_2O$ (**1**), $(UO_2)_4(PPA)_2(HPPA)_2{\cdot}Zn(H_2O)_6{\cdot}5H_2O{\cdot}$(**2**), $(UO_2)_2(H_2O)_2(PPA)_2Zn(H_2O)_4$ (**3**), and $(UO_2)_2(PPA)_2(HPPA)Zn_2(H_2O)_2{\cdot}3(H_2O)$ (**4**), adopt 1-, 2-, and 3-dimensional architectures wherein the UO_2^{2+} cation exhibits coordination preference for the phosphonate over the carboxylate oxygen atoms. The Zn^{2+} metal centers show an increased degree of ligand coordination with increasing reaction temperature. At 120 °C, compounds **1** and **2** are formed. These structures are 1- and 2-dimensional, respectively, and contain fully hydrated $[Zn(H_2O)_6]^{2+}$ cations. At 150 °C and 180 °C, the HPPA ligand displaces H_2O molecules from the inner Zn^{2+} hydration sphere and binds to the metal centers via a $-CO_2H$ oxygen atom in **3** and both carboxylate and phosphonate oxygen atoms in **4**. The overall Zn^{2+} reaction can be expressed by the equation $Zn(H_2O)_6^{2+}$ + HPPA ⇄ $Zn(H_2O)_5(HPPA)$ + H_2O. Presented here are the syntheses, structures, and characterization of these materials.

Introduction

Phosphonate ligands have historically played an important role in actinide separations due to the strong affinity of the phosphonate (-PO_3) group for the AnO_2^{2+} cation.[1–3] In spite of this relevance to separations and nuclear fuel stewardship, our knowledge of the structural chemistry of actinide phosphonates has largely been limited to those uranyl phenylphosphonates reported by Clearfield et al.,[4–12] as well as a handful of other compounds.[13–18] More recently, in an effort to probe the structural chemistry of uranyl phosphonate compounds and extend the known catalog of these materials beyond monophosphonates, the interaction of UO_2^{2+} with polyphosphonate[19–24] and carboxyphosphonate ligands[25–27] has been explored. These ligands are attractive candidates for materials synthesis due to the range of metal-to-ligand binding modes and the potential for novel structural topologies. Additionally, the heterofunctionality of phosphonocarboxylates provides a suitable forum to explore the syntheses of bimetallic uranium containing coordination polymers.

The coordination of UO_2^{2+} by carboxyphosphonate type species has also been explored within the context of understanding the behavior of uranium in biological and geological environments.[28–31] The migratory behavior of actinides in the environment is largely governed by factors such as E_H, pH, sorption onto mineral surfaces, coordination by organic matter and additionally interactions with microorganisms.[32,33] With respect to the latter, the interactions of biological species with uranium are influenced by the functionality of cellular components that include hydroxy, amino, phosphoryl, and carboxyl groups.[29,34] Carboxyphosphonate compounds contain functionalites analogous to those found in bacteria and other microorganisms, namely both phosphonate ($-PO_3$) and carboxylate ($-CO_2$) groups, and thus provide a suitable model for understanding the complexation behavior of actinides in bio-systems.[35] Whereas a number of UO_2^{2+}-carboxylate structures have been synthesized,[36–49] far fewer examples of solid-state UO_2^{2+}-carboxyphosphonate architectures have been reported.[25–27]

The interaction of UO_2^{2+} with bacterial cell-wall components, such as lipopolysaccharide, that contain high concentrations of phosphoryl and carboxyl groups has been explored in solution.[29] In these studies, the uranyl cation displayed coordination preference for the harder $-PO_3$ over the $-CO_2$ functionality. This is consistent with the coordination chemistry of the uranyl in the UO_2^{2+}-PPAs structures reported.[25–27] In fact, in the solid state, the propensity of the uranyl cation to bind preferentially to the phosphonate moieties over the carboxylate units was exploited by Albrecht-Schmitt et al. to construct a series of heterometallic UO_2^{2+}/Cu^{2+}/PPA compounds.[27] Beyond the bimetallic UO_2^{2+}/Cu^{2+} materials reported, however, the incorporation of other transition metal cations into UO_2^{2+}/PPA systems has not yet been explored. As such, we investigated reactions of uranium(VI) and triethyl phosphonoacetate in the presence of zinc under hydrothermal conditions. We herein report the synthesis, structure, and characterization

[a] Department of Chemistry, The George Washington University, 725 21st St. NW, Washington, DC 20052, USA
Fax: +1-202-994-5873
E-mail: cahill@gwu.edu

Supporting information for this article is available on the WWW under http://dx.doi.org/10.1002/ejic.200901080.

of four bimetallic UO_2^{2+}/Zn^{2+} carboxyphosphonates, $(UO_2)_2(PPA)_2(H_2O)_2{\cdot}Zn(H_2O)_6{\cdot}4H_2O$ (**1**), $(UO_2)_4(PPA)_2(HPPA)_2{\cdot}Zn(H_2O)_6{\cdot}5H_2O$ (**2**), $(UO_2)_2(H_2O)_2(PPA)_2Zn(H_2O)_4$ (**3**), and $(UO_2)_2(PPA)_2(HPPA)Zn_2(H_2O)_2{\cdot}3(H_2O)$ (**4**). The utility of in situ ester hydrolysis within the context of preparing these materials is also presented.

Results

Structure Description

Selected bond lengths and angles are listed in Table 1. Compound **1**, $(UO_2)_2(PPA)_2(H_2O)_2{\cdot}Zn(H_2O)_6{\cdot}4H_2O$, consists of UO_2O_5 monomers linked via phosphonoacetate units (Figure 1) to form chains of $[(UO_2)_2(PPA)_2(H_2O)_2]^{2-}$ that propagate along [100]. The pentagonal bipyramids shown in Figure 1 (b) are constructed from UO_2^{2+} cations equatorially bound to five oxygen atoms from three acid units and a bound water molecule (O5). The structure contains one crystallographically unique uranium metal center and one unique phosphonoacetate unit. Each PPA ligand is bound to one U^{VI} metal center in a bidentate fashion through phosphonate and carboxylate oxygen atoms (O3 and O4) at distances of 2.390(4) and 2.416(4) Å, respectively. The phosphonoacetate unit is bound to two additional U^{VI} metal centers in a monodentate manner through phosphonate oxygen atoms O6 and O7 with an average bond length of 2.344 Å. Hydrated $[Zn(H_2O)_6]^{2+}$ cations charge balance the anionic chains as shown in Figure 2.

Compound **2**, $(UO_2)_4(PPA)_2(HPPA)_2{\cdot}Zn(H_2O)_6{\cdot}5H_2O$, is constructed from four crystallographically unique U^{VI} metal centers and four unique PPA units as illustrated in Figure 3. Each U^{VI} site is characteristically bound to two axial oxygen atoms to form the UO_2^{2+} cation with an average U–O bond length of 1.7757 Å and an average O–U–O bond angle of 178.63°. Additionally, each UO_2^{2+} is equatorially bound to five oxygen atoms, which results in pentagonal bipyramid geometry. U(1) is coordinated to three phosphonoacetate units and one water molecule (O6). One acid unit, P(4)PA is bound in a bidentate fashion through phosphonate and carboxylate oxygen atoms, O7 and O3, at distances of 2.3537 and 2.4808 Å, respectively. Further, coordination of O3 to both U(1) and U(3) results in point-shared $(UO_2)_2O_9$ dimers which are linked via P(1)PA and P(4)PA into chains that extend along [1–10]. Additionally, coordination of carboxylate oxygen O21 to both U(2) and U(4) results in point-shared $U(2)O_2$–$U(4)O_2$ dimers that similarly propagate along [1–10] via P(2)PA and P(3)PA linkages. The two chains are connected along [001] via P(2)PA and P(4)PA to form the two-dimensional sheets illustrated in Figure 3. As shown in Figures 3 and 4, carboxylate oxygen atoms (O27–O30) from P(1)PA and P(3)PA are unbound and extend into the interlayer, which results in hydrogen-bonding interactions with O–H···O distances of 2.690 Å. $[Zn(H_2O)_6]^{2+}$ cations also reside in the interlayer and charge balance the anionic sheets.

Table 1. Selected bond lengths [Å] and angles [°] for **1**–**4**.

1[a]			
U(1)–O(1)	1.768(5)	O(4)–C(2)	1.283(8)
U(1)–O(2)	1.780(5)	O(8)–C(2)	1.251(8)
U(1)–O(4)	2.416(5)	C(1)–C(2)	1.506(9)
U(1)–O(5)	2.452(5)	Bond Angles	
U(1)–O(6)	2.353(4)	O(2)–U(1)–O(1)	179.2(2)
Zn(1)–O(10)	2.141(5)	$O(12)^1$–Zn(1)–O(12)	180.0(4)
Zn(1)–O(11)	2.080(5)	O(12)–Zn(1)–O(10)	91.24(19)
$P(1)–O(6)^3$	1.527(5)	O(12)–Zn(1)–O(11)	93.2(2)
P(1)–C(1)	1.810(6)		
2			
U(1)–O(1)	1.777(4)	O(3)–C(5)	1.290(6)
U(1)–O(2)	1.777(4)	O(16)–C(5)	1.246(6)
U(1)–O(3)	2.481(4)	C(5)–C(6)	1.501(7)
U(1)–O(6)	2.443(4)	Bond Angles	
U(1)–O(7)	2.354(3)	O(1)–U(1)–O(2)	178.86(18)
Zn(1)–O(40)	2.081(5)	O(24)–U(2)–O(8)	179.13(17)
Zn(1)–O(44)	2.038(6)	O(14)–U(3)–O(13)	178.93(18)
P(4)–O(7)	1.525(4)	O(26)–U(4)–O(19)	177.58(18)
P(4)–C(6)	1.809(5)		
3			
U(1)–O(1)	1.780(5)	C(1)–C(2)	1.523(10)
U(1)–O(2)	1.765(5)	O(4)–C(1)	1.242(9)
U(1)–O(3)	2.368(5)	O(15)–C(1)	1.261(8)
U(1)–O(4)	2.411(5)	Bond Angles	
U(1)–O(5)	2.556(5)	O(2)–U(1)–O(1)	177.5(2)
Zn(1)–O(15)	2.030(5)	O(9)–U(2)–O(8)	177.4(3)
Zn(1)–O(18)	2.205(6)		
P(1)–O(3)	1.519(5)		
P(1)–C(2)	1.808(7)		
4			
U(1)–O(1)	1.770(6)	C(5)–C(6)	1.486(11)
U(1)–O(2)	1.781(6)	O(4)–C(6)	1.268(9)
U(1)–O(3)	2.252(6)	O(7)–C(6)	1.271(10)
U(1)–O(4)	2.459(6)	Bond Angles	
U(1)–O(7)	2.637(6)	O(1)–U(1)–O(2)	178.7(3)
Zn(1)–O(20)	2.240(6)	O(8)–U(2)–O(9)	177.2(3)
Zn(2)–O(21)	2.013(6)		
$P(3)–O(3)^{10}$	1.518(6)		
P(3)–C(5)	1.813(8)		

[a] Symmetry transformations: (**1**) 1: $-x, -y, -z$; 3: $x + 1, y, z$. (**4**) 10: $-x + 1, -y + 1, -z + 1$.

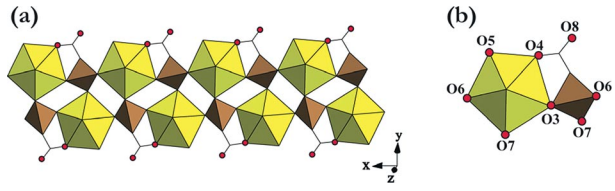

Figure 1. (a) Polyhedral representation of **1** illustrating $(UO_2)O_5$ monomers linked via phosphonoacetate ligands to form chains that propagate along [100]. Coordination to the U^{VI} metal centers occurs through both phosphonate and carboxylate oxygen atoms. (b) Illustration showing the local coordination of the U^{VI} site. Yellow polyhedra are uranium(VI) atoms in pentagonal bipyramid geometry. Brown polyhedra, black lines, and red circles represent the phosphorus, carbon, and oxygen atoms, respectively, of the phosphonoacetate ligand.

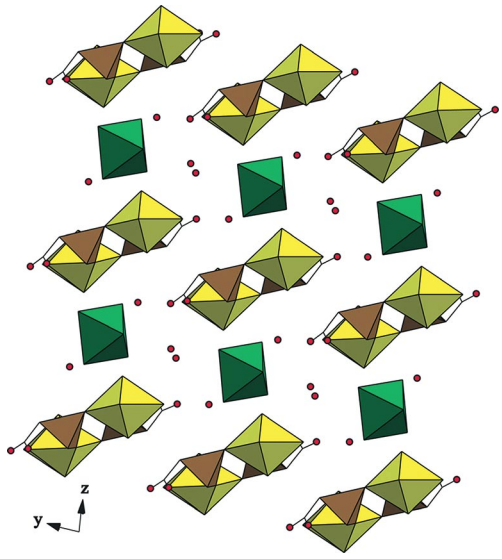

Figure 2. Packing diagram of **1** viewed down the [100] direction. Anionic chains of $[(UO_2)_2(PPA)_2(H_2O)_2]^{2-}$ are charged balanced by $[Zn(H_2O)_6]^{2+}$ cations. Green polyhedra represent hydrated Zn^{II} metal centers.

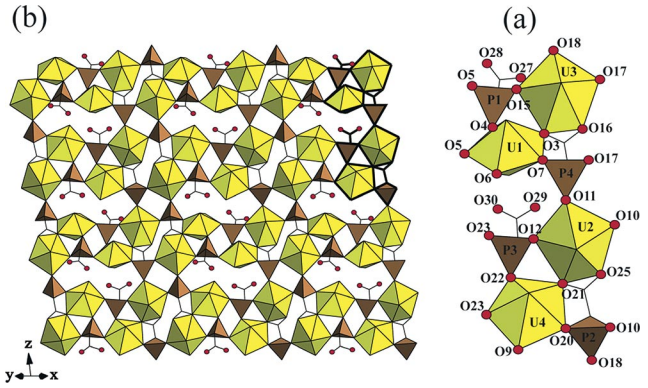

Figure 3. Polyhedral representation of **2** (a) illustrating the topology of the 2-dimensional sheets constructed from point-shared $(UO_2)O_9$ dimers linked via phosphonoacetate ligands. (b) Local coordination of each U^{VI} site. Coordination of P(2)PA and P(4)PA to the U^{VI} metal centers occurs through both phosphonate and carboxylate oxygen atoms, whereas coordination of P(1)PA and P(3)PA to the UO_2^{2+} sites occurs exclusively through phosphonate oxygen atoms. Bold lines in (a) represent highlighted section in (b).

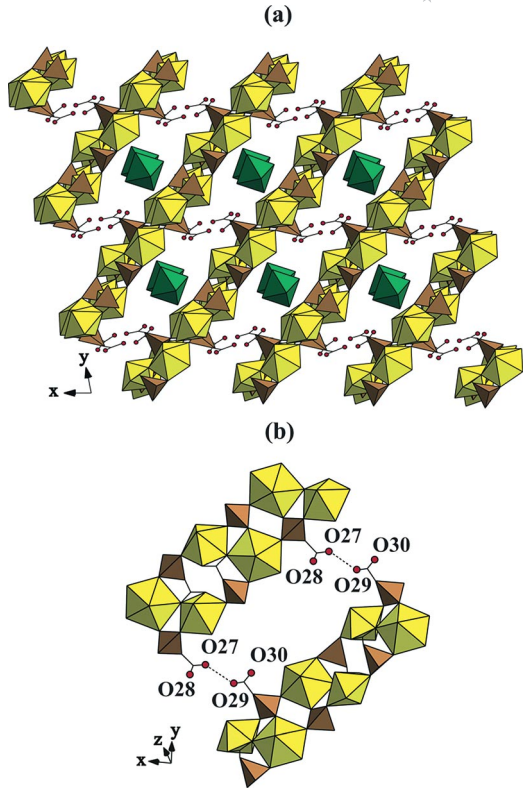

Figure 4. (a) View of **2** down the [001] direction illustrating the stacking of the uranium phosphonoacetate layers. Shown here, unbound carboxylate units protrude into the interlayer where hydrated Zn^{2+} cations reside. Solvent water molecules have been omitted for clarity. (b) Illustration of the hydrogen bonding interactions (2.690 Å) found in the interlayer of **2**.

Compound **3**, $(UO_2)_2(H_2O)_2(PPA)_2Zn(H_2O)_4$, consists of $UO_2(O_5)$ monomers linked through phosphonoacetate molecules to form chains that extend infinitely along [100] (Figure 5). Additional coordination of PPA carboxylate oxygen atoms to Zn^{2+} metal connects the chains along [010] into the 2-dimensional sheets shown in Figure 6, a. The structure is built from two crystallographically unique UO_2^{2+} sites, one unique Zn^{2+} metal center, and two unique phosphonoacetate units. U(1) is coordinated to two axial oxygen atoms (O1 and O2) at distances of 1.7647 and 1.7802 Å, respectively, to form the uranyl cation with a O_{Ur}–U–O_{Ur} bond angle of 177.52°. Further, U(1) is equatorially bound to five oxygen atoms, O3–O7, from three P(1) PA units and one bound water molecule (Figure 6). Two of the P(1)PA units are bound in a monodentate fashion via phosphonate oxygen atoms O6 and O7, whereas one P(1) PA molecule is coordinated to the U^{VI} metal center in a bidentate manner through phosphonate and carboxylate oxygen atoms O3 and O4, respectively. $U(2)O_2^{2+}$ is similarly coordinated in the equatorial plane to three P(2)PA ligands and a bound water molecule (O14). Two of the P(2)PA units are bound in a monodentate manner via phosphonate oxygen atoms O10 and O11, while one P(2)PA is bound in a bidentate fashion by phosphonate (O12) and carboxylate (O13) oxygen atoms. The Zn^{2+} metal center is coordinated

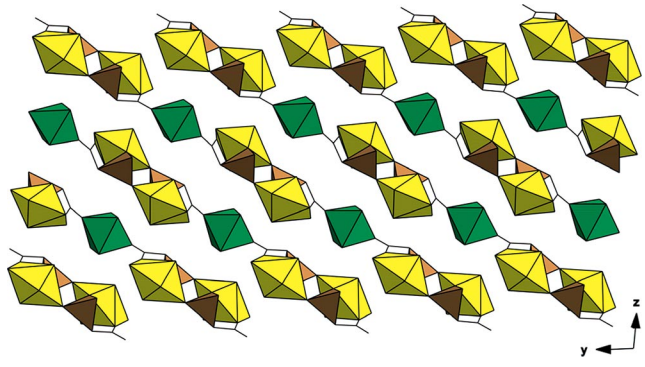

Figure 5. View of **3** down the [100] direction showing the stacking of the UO_2^{2+}/Zn^{2+}/PPA sheets.

to four water molecules (O17–O20) and two carboxylate oxygen atoms (O15 and O16), from two distinct PPA molecules, to form the octahedra shown in Figure 6, b.

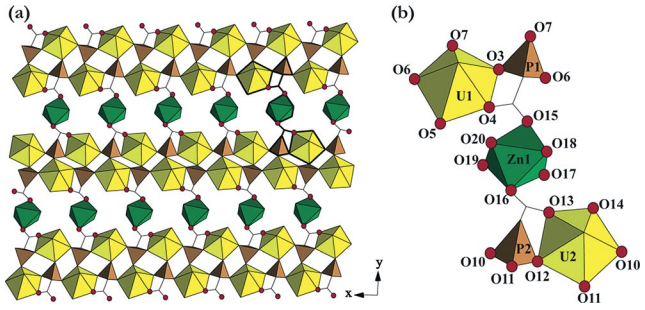

Figure 6. Illustration of **3** (a) viewed down the [001] direction depicting the topology of the 2D UO_2^{2+}/Zn^{2+}/PPA sheets and (b) showing the local coordination of the U^{VI} and Zn^{II} metal centers. Yellow polyhedra are uranium(VI) atoms in pentagonal bipyramid geometry, and green polyhedra are zinc(II) in octahedral geometry. Brown polyhedra, black lines, and red circles represent the phosphorus, carbon, and oxygen atoms, respectively, of the phosphonoacetate ligand. The bolded section in (a) is shown in (b).

Compound **4**, $(UO_2)_2(PPA)_2(HPPA)Zn_2(H_2O)_2{\cdot}3(H_2O)$ adopts a three-dimensional structure (Figure 8) and is built from two crystallographically unique UO_2^{2+} sites, three unique Zn^{2+} centers and three unique phosphonoacetate units (Figure 7). U(1)O_2^{2+} and U(2)O_2^{2+} are both equatorially coordinated to five oxygen atoms from four PPA ligands as shown in Figure 7 (a). Three of the PPA units are bound to each U^{VI} center in a monodentate fashion via phosphonate oxygen atoms, whereas one P(3)PA molecule is coordinated to the U^{VI} sites in a bidentate manner through phosphonate and/or carboxylate oxygen atoms. One P(3)PA unit binds to U(1) via carboxylate oxygen atoms O4 and O7 and is additionally bound to U(2) through phosphonate and carboxylate oxygen atoms O13 and O7, respectively. Coordination of P(3)PA to both U(1) and U(2) through carboxylate oxygen atom O7 results in point-shared $(UO_2)_2O_9$ dimers linked via P(3)PA units to form chains that propagate along [100]. P(3)PA additionally links U(2)O_2^{2+} monomers along [010] and coordination of P(1)PA and P(2)PA to chains of edge-shared Zn^{2+} octahedra that are polymerized along [010] results in the 3-dimensional structure depicted in Figure 8.

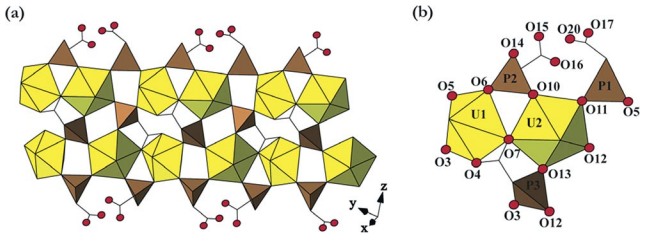

Figure 7. Polyhedral representation of **4** illustrating (a) the point-shared $(UO_2)O_9$ dimers linked along [100] via P(3)PA ligands and (b) the local coordination of each U^{VI} site. Coordination of P(1)PA and P(2)PA to the U^{VI} metal centers occurs exclusively through phosphonate oxygen atoms, whereas coordination of P(3)PA to the UO_2^{2+} sites occurs in a bidentate manner through phosphonate and carboxylate oxygen atoms.

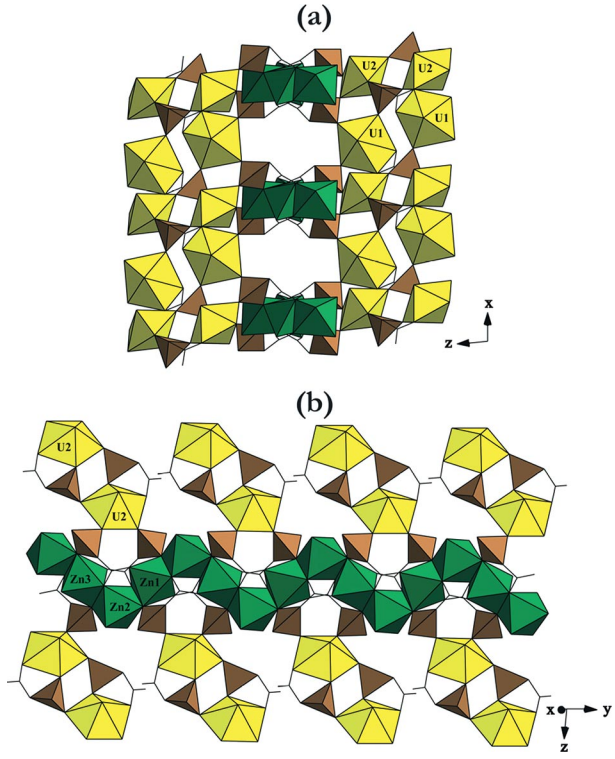

Figure 8. Illustration of **4** (a) viewed down the [010] direction depicting the UO_2^{2+}/PPA chains linked along [001] by coordination of PPA units to chains of Zn^{II} octahedra. (b) chains of the Zn^{II} metal centers polymerized along [010] that are subsequently linked to chains of U(2)O_2^{2+}/P(3)PA via P(1)PA and P(2)PA ligands. Yellow polyhedra are uranium(VI) atoms in pentagonal bipyramidal geometry, and green polyhedra are zinc(II) in octahedral geometry. Brown polyhedra, black lines, and red circles represent the phosphorus, carbon, and oxygen atoms, respectively, of the phosphonoacetate ligand. Solvent water molecules have been omitted for clarity.

Fluorescence Spectroscopy

The emission spectra for **1**–**4** exhibited the characteristic vibronic structure of the UO_2^{2+} cation with peaks ranging from 475 to 600 nm. The emission spectra for **1**–**4** are available in the Supporting Information (Figures S12–15).

Thermogravimetric Analysis

TGA curves for **1**–**4** can be found in the Supporting Information, Figures S16–19. A weight loss of 13% that can be attributed to the removal of surface water was observed when **1** was held at 50 °C for 30 min. Subsequent weight loss for **1** then occurred in three steps, the first of which (≈ 16%) took place between approximately 50 and 200 °C and is consistent with the loss of the solvent and bound water molecules from the structure. The final two steps occurred over 375–500 °C and 700–750 °C and resulted in

weight losses of ≈ 6% and ca. 3%, respectively; they are attributed to decomposition of the PPA ligands. The total weight loss for **2** was ca. 17% and occurred in four steps. An initial weight loss of 7% consistent with the loss of five lattice water molecules and two bound water molecules from the structure occurred between 50 and 100 °C. Loss of the two additional bound water molecules subsequently resulted in approximately 4% weight loss that was observed between 200 and 250 °C. The third step, attributed to the loss of the remaining water molecules occurred shortly thereafter and resulted in a weight loss of an additional 4–5%. Finally, a fourth weight loss consistent with the decomposition the $–CH_2$ moieties of the phosphonoacetate ligands began at 500 °C. The total weight loss for **3** was approximately 20%, and it occurred in four steps. Loss of bound water molecules (≈ 11%) began around 150 °C and was complete by 250 °C. Subsequent weight loss of an additional 9% resulting from decomposition of the phosphonoacetate units occurred in three consecutive steps over 400–750 °C. Weight loss for **4** occurred in two steps and resulted in a total loss of ca. 28%. The first step (≈ 17%) occurred over 50–200 °C and is consistent with the loss of five water molecules and decomposition of one PPA unit. Decomposition of the remaining PPA units resulted in a second weight loss of approximately 11% and occurred over 350–450 °C. The TGA curves for **1**–**4** are consistent with decomposition of the materials to multiple uranium and/or zinc phosphate such as $U_3(PO_4)_4$, $U_2P_2O_{10}$, $(UO)_2P_2O_7$, and $Zn_3(PO_4)_2$. TGA plots and PXRD data of **1** and **3** after thermal treatment are available in the Supporting Information.

Discussion

Reactions of UO_2^{2+}/Zn^{2+} and triethyl phosphonoacetate analogous to those yielding **1**–**4** were explored at room temperature, and after one month no crystals were obtained. Thus, hydrothermal conditions were used, and the phosphonoacetate ligand observed in the structures of **1**–**4** was generated through the hydrolysis of triethyl phosphonoacetate in situ. In light of these observations, one could speculate a kinetic contribution to these reactions wherein hydrolysis (and hence ligand availability) does not occur to an appreciable extent until such hydrolysis is promoted; in this case by temperature. In related transition metal systems, the hydrolysis of di- and trialkyl phosphonates has similarly been used to prepare a variety of transition metal carboxyphosphonates.[50–53] In these systems, the phosphonate ligands were generated in situ for the purpose of: (1) removing the need to synthesize the acid form of the ligand and (2) gradually introducing the ligand and thus yielding crystals sufficiently large for single-crystal X-ray diffraction.

The in situ generation of the phosphonoacetate ligand in this study presents an additional benefit. That is, efforts to prepare UO_2^{2+}/Zn^{2+} bimetallic materials by direct reaction of the metal cations with phosphonoacetic acid under hydrothermal conditions have been unsuccessful. In fact, reactions comparable to those presented herein wherein phosphonoacetic acid was used in place of triethylphosphonoacetate yielded a previously reported, homometallic material, $UO_2(HPPA)$.[25] Taking the acidity of these systems into account, reactions of UO_2^{2+}, Zn^{2+}, and phosphonoacetate at pH 4–5 were also explored; pH was adjusted with NH_4OH. After six days at 120, 150, and 180 °C, a biphasic sample containing a known homometallic UO_2^{2+} phosphonoacetate, $(UO_2)(O_3PCH_2CO_2)\cdot NH_4\cdot H_2O$, and various uranium oxide/hydroxides was obtained.

The hydrolysis of triethyl phosphonoacetate to yield PPA also generates three equivalents of EtOH. Thus, reactions of UO_2^{2+}, Zn^{2+}, phosphonoacetate, and ethanol in H_2O at room temperature and 120 °C were also explored. These reactions have been found to yield bimetallic products, including **1** and **2** as well as an additional bimetallic phase at 120 °C, further characterization of which is in progress. That said, the differences in product formation by in situ ligand formation vs. direct assembly observed in this system may be attributed to the ethanol generated in situ by ester hydrolysis. In the presence of ethanol, for instance, the hydrogen bonding networks that stabilize many metal phosphonates including the homometallic $UO_2(HPPA)$ phase mentioned previously may be disrupted such that more favorable conditions for the incorporation of transition metal cations into the interlayer are present. The ethanol generated by means of in situ ester hydrolysis may also affect the dielectric constant of the solvent system, albeit to a limited extent, given it would constitute less than 1% of the total solvent. In any case and even though ethanol is not observed in the crystalline reaction product, it is conceivable that it influences product formation by altering the hydrogen-bonding networks or otherwise affecting solubility. Theses results are consistent with previous findings wherein spectator species, charge balancing countercations, and organic diamines were found to influence product formation to some extent.[25,26]

Compounds **1**–**4** exhibit structural features and trends consistent with the UO_2^{2+}-PPAs reported. All are constructed from $UO_2(O_5)$ pentagonal bipyramids linked via phosphonoacetate units. Additionally, the UO_2^{2+} coordinates preferentially to the $–PO_3$ oxygen atoms as predicted by HSAB theory.[54] Despite these similarities, however, **1**–**4** exhibit remarkably different structures both in terms of topology and dimensionality. Such differences can be attributed to oligomerization of the metal centers and metal–ligand binding modes, both for the UO_2^{2+} and Zn^{2+} metal centers. Compounds **1** and **3** contain discrete UO_2^{2+} monomers bound to three phosphonate ligands and one water molecule to result in $[(UO_2)_2(PPA)_2(H_2O)_2]^{2-}$ chains. These anionic units resemble those found in $[AnO_2(TO_4)(H_2O)_2\cdot nH_2O]$ (T = S, Se, Mo, Cr) architectures,[55] yet one of the bound H_2O molecules is replaced by a carboxylate oxygen atom from the PPA unit in **1** and **3**. As the carboxylate and H_2O molecules do not play a role in linking the UO_2^{2+} building units, the fundamental topology of these structures is analogous. Compounds **1** and **3** do, however, differ with respect to dimensionality. Whereas **1** contains 1-dimen-

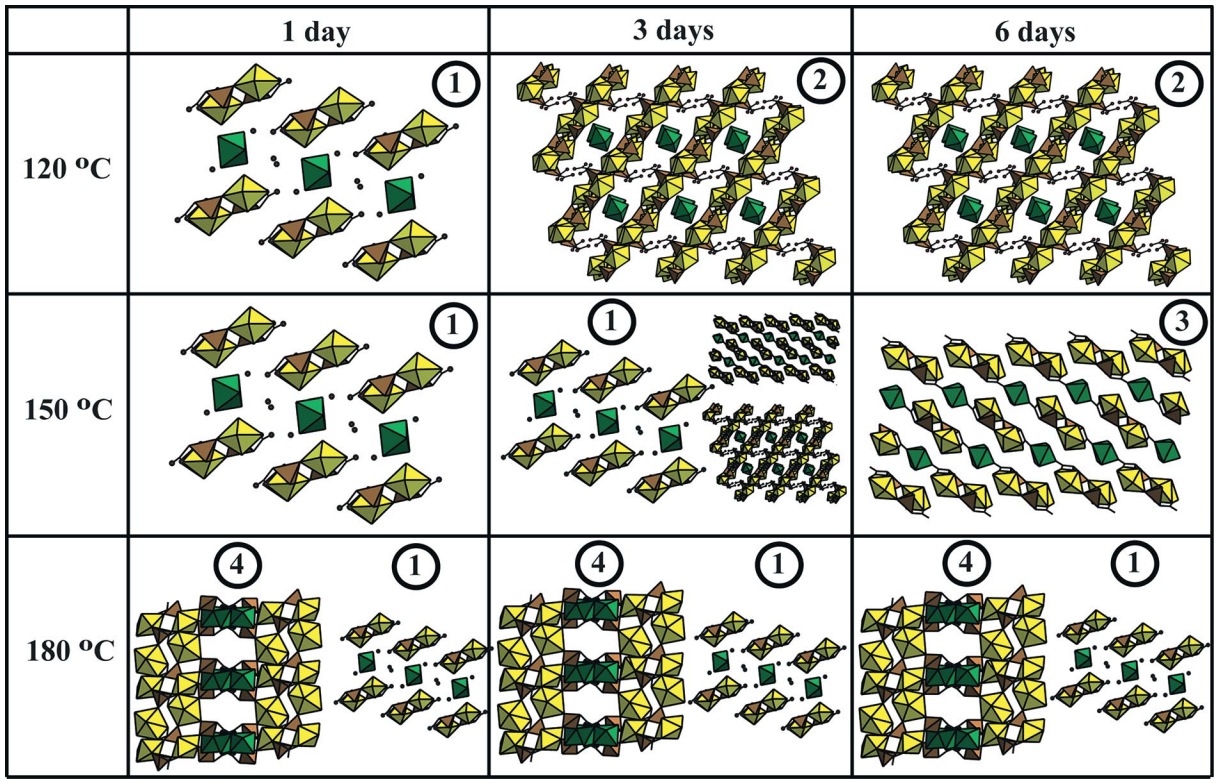

Figure 9. Polyhedral representation of the phases prepared at 120, 150, and 180 °C as a function of time. Dominant phases are labeled.

sional chains, **3** adopts a 2-dimensional structure, resulting from coordination of the unbound carboxylate oxygen atom in **1** to a Zn^{2+} metal center in **3**. Note that the Zn^{2+} metal centers in **1** exist in their fully hydrated form as $[Zn(H_2O)_6]^{2+}$ units. Interestingly, compound **1** can be synthesized as a pure phase at 120 °C and 150 °C over one day. After six days at 150 °C, compound **3** can be synthesized as a pure phase. Thus at 150 °C, aging of the system seemingly promotes Zn^{2+}-PPA coordination. These results are summarized in Figure 9.

Compounds **2** and **4** alternatively contain point-shared $(UO_2)_2(O)_9$ dimers that are connected by PPA units to form 2- and 3-dimensional structures, respectively. Each UO_2^{2+} site is ligated by four phosphonate ligands, three in a monodentate manner and one in a bidentate fashion. In both cases, the dimers result from the coordination of a carboxylate oxygen atom to two UO_2^{2+} metal centers. Though **2** and **4** share many structural features, their overall architectures are strikingly different. This is in part realized by increased coordination of the Zn^{2+} metal centers, observed in **4** as compared to **2**. In **2**, the Zn^{2+} sites exist as discrete $[Zn(H_2O)_6]^{2+}$ units. These fully hydrated Zn^{2+} species are similarly found in the structure of **1**; both **1** and **2** can be synthesized at 120 °C. At 180 °C, however, increased coordination of the phosphonoacetate to the Zn^{2+} sites and polymerization of the Zn^{2+} into chains of Zn^{2+} octahedra is observed.

In comparing the six-day reactions at 120, 150, and 180 °C, an evolution of metal–ligand coordination and dimensionality is present. The coordination environment of the UO_2^{2+} metal center and the presence of monomers vs. dimers as a function of temperature and reaction time is not entirely apparent, yet in looking at the inner coordination sphere of the Zn^{2+} metal centers illustrated in Figure 10, a trend is clear. As reaction temperature increases, Zn^{2+}–PPA coordination also increases. Whereas fully hydrated Zn^{2+} are observed at 120 °C, $Zn(H_2O)_4(PPA)_2$ are present at 150 °C, and $Zn(H_2O)_2(PPA)_4$ and $Zn(PPA)_6$ units are seen at 180 °C. The overall reaction can thus be expressed as $Zn(H_2O)_6^{2+}$ + HPPA ⇔ $Zn(H_2O)_5(HPPA)$ + H_2O wherein inner sphere H_2O molecules are increasingly displaced by oxygen atoms from the PPA units with increasing reaction temperature.

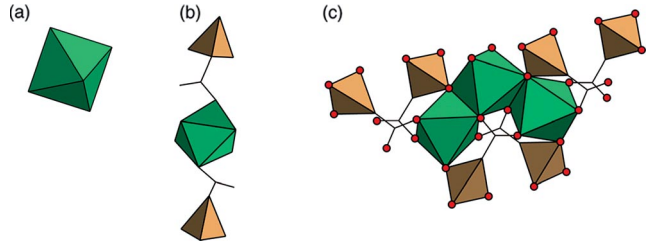

Figure 10. Polyhedral representation of the local coordination environment of the Zn^{2+} metal centers at (a) 120 °C, (b) 150 °C, and (c) 180 °C. Green polyhedra are zinc(II) in octahedral geometry. Brown polyhedra, black lines, and red circles represent the phosphorus, carbon, and oxygen atoms of the phosphonoacetate ligand.

The reaction products were also explored as a function of reaction time; the results are summarized in Figure 9. Interestingly compound **1** is present in the products from

reactions at 120, 150, and 180 °C and persists over different lengths of times. After evaporation of a solution obtained from a one-day reaction at 120 °C, compound **1** is obtained as a microcrystalline powder. After three/six days at 120 °C, however, compound **2** is isolated. Both contain $[Zn(H_2O)_6]^{2+}$ cations. Compound **1** contains discrete $UO_2(O_5)$ monomers, whereas **2** consists of $UO_2(O)_9$ dimers. Here, aging of the system results in oligomerization of the UO_2^{2+} sites. As previously mentioned, compound **1** also precipitates from reactions at 150 °C over one and three days. After six days, **3** is obtained in pure phase. In this case, aging of the reaction results in increased Zn^{2+}–PPA coordination. At 180 °C over one, three, and six days **1** and **4** are obtained in varying yield. The presence of **4** at the higher temperature is consistent with the metal–ligand coordination trends already discussed, whereas the presence of **1**, and in particular $[Zn(H_2O)_6]^{2+}$ cations at 180 °C, may perhaps speak for the stability of that phase. In other words, phase stability, as evidenced by **1**, competes with the tendency of the metal cations to polymerize, and also, in the case of Zn^{2+} specifically, coordinate to the PPA ligand.

Conclusions

In summary, four novel bimetallic uranium phosphonoacetates have been prepared under hydrothermal conditions by the in situ hydrolysis of triethylphosphonoacetate. Efforts to prepare the bimetallic materials from the direct reaction of the metal salts with the acid form of the ligand were unsuccessful and thus demonstrate the utility of in situ reactions as an alternative synthetic approach. These compounds are all similarly built from UO_2^{2+} pentagonal bipyramids yet exhibit markedly diverse topologies and dimensionality, adopting 1-, 2-, and 3-dimensional architectures. These differences can be attributed to polymerization of UO_2^{2+} sites in **2** and **4** to form $(UO_2)_2O_9$ dimers, oligomerization of Zn^{2+} octahedra in **4**, and increased Zn^{2+}–ligand coordination as observed in **3** and **4**. With respect to the Zn^{2+} metal centers, increased metal–ligand coordination is observed with increasing temperature.

Experimental Section

Caution: The uranium oxynitrate used in this investigation contains depleted uranium, yet standard precautions for handling radioactive substances should be followed.

Syntheses: Compounds **1**–**4** were synthesized hydrothermally as outlined in Table 2. The reactants were placed into a 23-mL Teflon-lined Parr bomb that was then sealed and heated statically in an isothermal oven. (1) After one day at 120 °C, the reaction vessel was removed from the oven and placed on the benchtop to cool over four hours. Upon cooling to room temperature, a clear yellow solution was obtained. The solution was allowed to evaporate at room temperature and after two days a yellow solid was obtained. Note that compound **1** can also be prepared at 150 °C over one or three days. (2) After three or six days at 120 °C, a clear yellow solution was decanted and yellow crystals were obtained. The crystals were washed with distilled water and ethanol and then allowed to air dry at room temperature. (3) After six days at 150 °C, a clear yellow solution was decanted and yellow crystals were obtained. The crystals were washed with distilled water and ethanol and allowed to air dry at room temperature. Note that at 150 °C over one or three days, compounds **1** and **3** were present in the reaction product in varying yield. (4) After one, three, or six days at 180 °C compounds **1** and **4** were obtained from a mixed product and were present in varying yield. Powder X-ray diffraction data of the reaction products at 120, 150, and 180 °C over one, three, and six days are available in the Supporting Information, Figures S1–S3.

X-ray Structure Determination: A single crystal from each of the samples was isolated from the product and mounted on a glass fiber. Reflections were collected with a Bruker SMART diffractometer equipped with an APEX II CCD detector using Mo-K_α radiation and a combination of 0.5° ω and ϕ scans. The data were integrated and corrected for absorption using the Apex2 suite of crystallographic software.[56] All compounds were solved by direct methods and refined using SHELXL-97[57] within the WinGX

Table 2. Synthetic details for **1**–**4**.

	1	**2**	**3**	**4**
$(UO_2)(NO_3)_2{\cdot}6H_2O$	0.143 g (0.30 mmol)	0.149 g (0.30 mmol)	0.139 g (0.28 mmol)	0.141 g (0.28 mmol)
$Zn(NO_3)_2{\cdot}6H_2O$	0.089 g (0.30 mmol)	0.093 g (0.31 mmol)	0.085 g (0.29 mmol)	0.089 g (0.30 mmol)
teppa	0.120 mL (0.60 mmol)	0.120 mL (0.60 mmol)	0.120 mL (0.60 mmol)	0.120 mL (0.60 mmol)
H_2O	4 g (224 mmol)	4 g (224 mmol)	4 g (224 mmol)	4 g (224 mmol)
Molar ratios	1:1:2:640	1:1:2:640	1:1:2:640	1:1.1:2:640
pHi, pHf	2.0, 1.9	2.0, 1.7	2.1, 2.1	2.2, 2.2
Temperature [°C]	120	120	150	180
Time [d]	1	6	6	6
Crystal color	Green-yellow	yellow	yellow	yellow
Crystal habit	needle	plate	needle	plate
Yield (based on U)	20%	54%	41%	45%
EA[a] Obsd. (Calcd.)	C 4.45% (4.38%) H 2.62% (2.58%)	C 4.95% (4.97%) H 1.76% (1.88%)	C 4.83% (4.86%) H 1.45% (1.63%)	C 6.14% (6.14%) H 1.41% (1.46%)

[a] Elemental Analysis (EA) by combustion, Galbraith Laboratories, Knoxville, TN. As **4** could not be prepared as a pure phase, the EA results reported reflect those observed for a sample wherein single crystals of **4** were isolated from the bulk reaction product. This sample was used in all subsequent characterization of **4** including TGA and FLR.

Table 3. Crystallographic data and structure refinement for **1**–**4**.

	1	**2**	**3**	**4**
Empirical formula	$C_4H_{28}O_{26}P_2U_2Zn$	$C_8H_{36}O_{41}P_4U_4Zn$	$C_4H_{16}O_{20}P_2U_2Zn$	$C_6H_{17}O_{24}P_3U_2Zn_2$
Fw	1095.63	1929.74	987.54	1172.91
Temperature [K]	100	100	295	295
λ (Mo-K_α)	0.71073	0.71073	0.71073	0.71073
Crystal system	triclinic	triclinic	triclinic	triclinic
Space group	$P\bar{1}$	$P\bar{1}$	$P\bar{1}$	$P\bar{1}$
a [Å]	7.0298(7)	10.6675(3)	6.9444(5)	9.1030(10)
b [Å]	8.2499(8)	11.5380(3)	8.3707(6)	9.7275(11)
c [Å]	10.9824(11)	17.2140(4)	16.0483(11)	15.0950(17)
α [°]	81.182(2)	78.4650(4)	97.541(1)	91.404(2)
β [°]	74.143(2)	87.5517(4)	96.433(1)	94.497(2)
γ [°]	89.902(2)	76.3111(4)	91.798(1)	115.628(2)
V [Å^3]	604.91(10)	2016.94(9)	917.98(11)	1198.9(2)
Z	1	2	2	2
$D_{calcd.}$ [g cm^{-3}]	3.008	3.177	3.573	3.249
μ [mm^{-1}]	14.579	16.872	19.169	15.749
R_{int}	0.0548	0.0367	0.0445	0.0617
R_1[a] [$I > 2\sigma(I)$]	0.0280	0.0282	0.0266	0.0373
wR_2[a]	0.0592	0.0713	0.0491	0.0932

[a] $R_1 = \Sigma \, ||F_o| - |F_c|| / \Sigma |F_o|$; $wR_2 = \{\Sigma[w(F_o^2 - F_c^2)^2] / \Sigma[w(F_o^2)^2]\}^{1/2}$.

software suite.[58] Satisfactory refinements as well as tests for missing symmetry, using Platon,[59] indicated that no obvious space group changes were needed or suggested. Crystallographic data for **1**–**4** are provided in Table 3.

CCDC-743317 (for **1**), -743318 (for **2**), -743319 (for **3**), -743320 (for **4**) contain the supplementary crystallographic data for this paper. These data can be obtained free of charge from The Cambridge Crystallographic Data Centre via www.ccdc.cam.ac.uk/data_request/cif.

All non-hydrogen atoms were located using difference Fourier maps and were ultimately refined anisotropically. Hydrogen atoms of the phosphonoacetate $-CH_2$ groups were placed in calculated positions and bond lengths were fixed at 0.97 Å. Hydrogen atoms of the lattice water molecules or bound water molecules in **1**–**4** were not found during refinement. While hydrogen atoms of the –COOH moieties in **1** were located in difference Fourier maps and placed in calculated positions, those in **4** were not located during refinement.

Powder X-ray diffraction data were collected for **1**–**4** using a Rigaku Miniflex diffractometer (Cu-K_α, 3–60°) and manipulated using the JADE software package.[60] As compound **4** was not obtained as a pure phase, single crystals were manually isolated from the reaction product and powder X-ray diffraction data were collected on that sample. Agreement between the calculated and observed patterns shown in Figures S4–7 suggest that the single crystals used for structure determination were representative of the bulk sample (with the exception of **4**).

Characterization: Thermogravimetric analysis (TGA) was performed with either a Perkin–Elmer Pyris1 or a TA Instruments Q5000 instrument at a rate of 10 °C/min under flowing nitrogen gas. To remove surface water, **1** and **4** were held at 50 °C for 30 min, after which the sample was heated to 800 °C. Emission spectra were collected with a Shimadzu RF-5301 PC Spectrofluorophotometer [uranium excitation wavelength 365 nm; emission wavelength: 450–600 nm; slit width: 1.5 nm (excitation) and 1.5 nm (emission); sensitivity: high with a UV-35 filter].

Supporting Information (see also the footnote on the first page of this article): ORTEP illustrations of **1**–**4** as well as all TGA plots, PXRD data, and FLR spectra.

Acknowledgments

Major support for this work is from The National Science Foundation (NSF) (DMR-0348982 and DMR-0419754). Additional funding (KEK) is provided as part of the Materials Science of Actinides, an Energy Frontier Research Center funded by the U.S. Department of Energy, Office of Science, Office of Basic Energy Sciences under Award Number DE-SC0001089. We are grateful to Sayon A. Kumalah and Stephen Drake (Georgetown University) for TGA data of **1** and **4**. KEK also gratefully acknowledges the ARCS (Achievement Reward for College Scientists) Foundation, Metro Washington Chapter for their support.

[1] K. L. Nash, *J. Alloys Compd.* **1994**, *213–214*, 300–304.
[2] K. L. Nash, *J. Alloys Compd.* **1997**, *249*, 33–40.
[3] M. P. Jensen, J. V. Beitz, R. D. Rogers, K. L. Nash, *J. Chem. Soc., Dalton Trans.* **2000**, *18*, 3058–3064.
[4] A. Clearfield, in: *Progress in Inorganic Chemistry* (Ed.: K. D. Karlin), John Wiley & Sons, New York, **1998**, vol. 47, pp. 371–510.
[5] D. Grohol, A. Clearfield, *J. Am. Chem. Soc.* **1997**, *119*, 4662–4668.
[6] D. Grohol, A. Clearfield, *J. Am. Chem. Soc.* **1997**, *119*, 9301–9302.
[7] D. Grohol, F. Gingl, A. Clearfield, *Inorg. Chem.* **1999**, *38*, 751–756.
[8] M. A. G. Aranda, A. Cabeza, S. Bruque, D. M. Poojary, A. Clearfield, *Inorg. Chem.* **1998**, *37*, 1827–1832.
[9] D. M. Poojary, A. Cabeza, M. A. G. Aranda, S. Bruque, A. Clearfield, *Inorg. Chem.* **1996**, *35*, 1468–1473.
[10] D. M. Poojary, D. Grohol, A. Clearfield, *Angew. Chem. Int. Ed. Engl.* **1995**, *34*, 1508–1510.
[11] D. M. Poojary, D. Grohol, A. Clearfield, *J. Phys. Chem. Solids* **1995**, *56*, 1383–1388.
[12] D. Grohol, M. A. Subramanian, D. M. Poojary, A. Clearfield, *Inorg. Chem.* **1996**, *35*, 5264–5271.
[13] M. B. Doran, A. J. Norquist, D. O'Hare, *Chem. Mater.* **2003**, *15*, 1449–1455.
[14] W. Henderson, M. T. Leach, B. K. Nicholson, A. L. Wilkins, t. l. P. A. T. Hoye, *Polyhedron* **1998**, *17*, 3747–3752.
[15] D. T. Cromer, R. R. Ryan, S. Karthikeyan, R. T. Paine, *Inorg. Chim. Acta* **1990**, *172*, 165–172.

[16] S. Karthikeyan, R. T. Paine, R. R. Ryan, *Inorg. Chim. Acta* **1988**, *144*, 135–141.
[17] A. Cabeza, M. A. G. Aranda, F. M. Cantero, D. Lozano, M. Martinez-Lara, S. Bruque, *J. Solid State Chem.* **1996**, *121*, 181–189.
[18] M. B. Dines, P. C. Griffith, *Polyhedron* **1983**, *2*, 607–611.
[19] S.-S. Bao, G.-S. Chen, Y. Wang, Y.-Z. Li, L.-M. Zheng, Q.-H. Luo, *Inorg. Chem.* **2006**, *45*, 1124–1129.
[20] A.-G. D. Nelson, T. H. Bray, T. E. Albrecht-Schmitt, *Angew. Chem. Int. Ed.* **2008**, *47*, 6252–6254.
[21] A.-G. D. Nelson, T. H. Bray, F. A. Stanley, T. E. Albrecht-Schmitt, *Inorg. Chem.* **2009**, *48*, 4530–4535.
[22] A.-G. D. Nelson, T. H. Bray, W. Zhan, R. G. Haire, T. S. Sayler, T. E. Albrecht-Schmitt, *Inorg. Chem.* **2008**, *47*, 4945–4951.
[23] P. O. Adelani, T. E. Albrecht-Schmitt, *Inorg. Chem.* **2009**, *48*, 2732–2734.
[24] A. A. Russell, R. L. Meline, E. N. Duesler, R. T. Paine, *Inorg. Chim. Acta* **1995**, *231*, 1–5.
[25] K. E. Knope, C. L. Cahill, *Inorg. Chem.* **2008**, *47*, 7660–7672.
[26] K. E. Knope, C. L. Cahill, *Inorg. Chem.* **2009**, *48*, 6845–6851.
[27] A. N. Alsobrook, W. Zhan, T. E. Albrecht-Schmitt, *Inorg. Chem.* **2008**, *47*, 5177–5183.
[28] A. Koban, G. Bernhard, *J. Inorg. Biochem.* **2007**, *101*, 750–757.
[29] A. Barkleit, H. Moll, G. Bernhard, *Dalton Trans.* **2008**, 2879–2886.
[30] M. Gavrilescu, L. V. Pavel, I. Cretescu, *J. Hazard. Mater.* **2009**, *35*, 163.
[31] N. Renninger, R. Knopp, H. Nitsche, D. S. Clark, J. D. Keasling, *Appl. Environ. Microbiol.* **2004**, *70*, 7404–7412.
[32] G. R. Choppin, *J. Nucl. Radiochem. Sci.* **2005**, *6*, 1–5.
[33] L. Soderholm, S. Skanthakumar, D. Gorman-Lewis, M. P. Jensen, K. L. Nagy, *Geochim. Cosmochim. Acta* **2008**, *72*, 140–150.
[34] J. D. Van Horn, H. Huang, *Coord. Chem. Rev.* **2006**, *250*, 765–775.
[35] Z. Cao, K. Balasubramanian, M. G. Calvert, H. Nitsche, *Inorg. Chem.* **2009**, *48*, 9700–9714.
[36] J. M. Harrowfield, N. Lugan, G. H. Shahverdizadeh, A. A. Soudi, P. Thuery, *Eur. J. Inorg. Chem.* **2006**, 389–396.
[37] L. A. Borkowski, C. L. Cahill, *Cryst. Growth Des.* **2006**, *6*, 2241–2247.
[38] L. A. Borkowski, C. L. Cahill, *Cryst. Growth Des.* **2006**, *6*, 2248–2259.
[39] C. L. Cahill, L. A. Borkowski, in: *Structural Chemistry of Inorganic Actinide Compounds* (Eds.: S. V. Krivovichev, P. C. Burns, I. G. Tananaev), Elsevier, Amsterdam, **2007**, p. 419.
[40] M. Frisch, C. L. Cahill, *Dalton Trans.* **2005**, 1518–1523.
[41] K. E. Knope, C. L. Cahill, *Inorg. Chem.* **2007**, *46*, 6607–6612.
[42] B. Masci, P. Thuery, *CrystEngComm* **2008**, *10*, 1082–1087.
[43] P. Thuery, *Polyhedron* **2007**, *26*, 101–106.
[44] P. Thuery, *CrystEngComm* **2009**, *11*, 232–234.
[45] W. Chen, H.-M. Yuan, J.-Y. Wang, Z.-Y. Liu, J.-J. Xu, M. Yang, J.-S. Chen, *J. Am. Chem. Soc.* **2003**, *125*, 9266–9267.
[46] P. A. Giesting, P. C. Burns, N. J. Porter, *Mater. Res. Soc. Symp. Proc.* **2006**, *893*, 399–404.
[47] L. Duvieubourg, G. Nowogrocki, F. Abraham, S. Grandjean, *J. Solid State Chem.* **2005**, *178*, 3437–3444.
[48] Y.-S. Jiang, Z.-T. Yu, Z.-L. Liao, G.-H. Li, J.-S. Chen, *Polyhedron* **2006**, *25*, 1359–1366.
[49] Y.-Z. Zheng, M.-L. Tong, X.-M. Chen, *Eur. J. Inorg. Chem.* **2005**, 4109–4117.
[50] P.-A. Jaffrès, D. Villemin, V. Caignaert, *Chem. Commun.* **1999**, 1997.
[51] J.-J. Hou, X.-M. Zhang, *Cryst. Growth Des.* **2006**, *6*, 1445–1452.
[52] G. B. Hix, B. M. Kariuki, S. Kitchin, M. Tremayne, *Inorg. Chem.* **2001**, *40*, 1477–1481.
[53] X.-M. Zhang, *Eur. J. Inorg. Chem.* **2004**, 544–548.
[54] R. G. Pearson, *J. Chem. Educ.* **1968**, *45*, 581–587.
[55] S. V. Krivovichev, P. C. Burns, in: *Structural Chemistry of Inorganic Actinide Compounds* (Eds.: S. V. Krivovichev, P. C. Burns, I. G. Tananaev), Elsevier, Amsterdam, **2007**, pp. 95–182.
[56] Bruker, Bruker AXS, Madison, WI, **2008**.
[57] G. Sheldrick, *Acta Crystallogr., Sect. A* **2008**, *64*, 112–122.
[58] L. Farrugia, *J. Appl. Crystallogr.* **1999**, *32*, 837–838.
[59] A. L. Spek, *Acta Crystallogr., Sect. A* **1990**, *46*, C34.
[60] *JADE*, v. 6.1ed., Materials Data Inc., Livermore, CA, **2002**.

Received: November 5, 2009
Published Online: January 29, 2010

